

Facile synthesis of Co-Ni-Mn oxide for high performance supercapacitor

Qingli Sui, Cuili Xiang*, Yongjin Zou, Erhu Yan, Huangzhi Zhang, Fen Xu, Lixian Sun*

Guangxi Key Laboratory of Information Materials, Guilin University of Electronic Technology, Guilin 541004, P.R. China

*E-mail: xiangcuili@guet.edu.cn; sunlx@guet.edu.cn

Received: 5 July 2019 / Accepted: 4 September 2019 / Published: 29 October 2019

Transition metal oxides possess unique properties for energy storage devices. In this study, Co-Ni-Mn ternary metal oxide (Co-Ni-Mn-O) was synthesized in a facile way. Co-Ni alloy was first prepared by chemical reduction and then oxidized by potassium permanganate. MnO₂ was thus covered on the Co-Ni oxides. The Co-Ni-Mn-O has high electrochemical activity and can be used for supercapacitor electrode. The Co-Ni-Mn-O demonstrates high specific capacitance as well as excellent rate capability and stability, which is promising for energy storage applications.

Keywords: MnO₂; Supercapacitor; Transition metal oxides; Ternary metal oxide; Nanocomposite

1. INTRODUCTION

The energy crisis enables people to look for renewable energy to replace fossil fuel. However, the well-known renewable energies such as solar energy, wind energy are unstable. They need to be stored and released in a controlled way [1-3]. Therefore, the energy storage devices have received considerable attention in recent years [4-9]. Compared with Li-ion battery, supercapacitor possesses higher power density, lower price, faster charging rate and longer stability [10]. However, the low energy density of supercapacitor limits its wide application. The conventional materials used in the supercapacitor are carbon-based material. The capacitance of the carbon material is less than 400 F g⁻¹. Therefore, the search for high performance is urgent need. In the past decades, scientists found that transition metal oxides, conducting polymer can store charges through Faradic reaction [11-14], which is so called pseudo-capacitive materials. The specific capacitance of this type of materials can reach up to 3000 F g⁻¹ if the materials are rational designed. Therefore, different type of pseudo-capacitive materials has been extensively studied.

Transition metal oxides such as Co, Mo oxides, possess super high theoretical capacitance

value. For instance, the theoretical capacitances for CoO and NiO are 4292 and 2584 F g⁻¹, respectively [15]. The combination of two or more transition metal oxides together can potentially reduce the inner resistance of the material and improve the stability of the materials due to the synergistic effects [16-18]. Furthermore, the potential windows of the supercapacitor can be effectively enlarged [19]. The binary oxides such Ni-Co, Ni-Mn, Co-Mn oxides have been well studied [20-22]. However, the ternary oxide of Co-Ni-Mn was rarely reported. In this study, Co-Ni-Mn was prepared in a facile way. Co-Ni alloy can be easily obtained from the solution by chemical reduction. The Co-Ni alloy is high active prepared in this way, which is always used as the catalyst for hydrogen generation [23]. On the other hand, potassium permanganate has high oxidative potential, which can potentially oxidize the Co-Ni alloy and form Mn oxides on the surface Co-Ni oxides at same time. Based on this concept, the Co-Ni-Mn oxide was prepared. The obtained the Co-Ni-Mn oxide was characterized by physicochemical methods and electrochemical measurements in detail.

2. MATERIALS AND METHODS

2.1. Synthesis of Co-Ni-Mn-O

Chemicals used in this study are from commercial sources and analytical grade. A typical procedure to prepare Co-Ni-Mn oxide is as follow: 1 g of CoSO₄ and 0.5 g of NiSO₄ were dissolved in 100 mL acetonitrile under stirring. Then a solution (10 mL) containing 2 g of NaBH₄ was added to the above solution dropwise. The mixture was stirred for 2 h. Next, the solution was filtered and the black solid was washed and dried. The power was denoted as Co-Ni-B. Then 0.1 g of Co-Ni-B was dispersed in 10 mL potassium permanganate (0.001 M) and stirred for 2 h. The solid was centrifuged and wash several times with distilled water. Finally, the sample was dried in an oven for 6 h. The sample was denoted as Co-Ni-Mn-O.

2.2. Characterization

The samples were characterized with scanning electron microscopy (SEM, QUANTA200), Transmission electron microscope (TEM, Tecnai G2 F20) images, Powder X-ray diffraction (XRD, D8 Advance), X-ray photoelectron spectroscopy (XPS, ESCA250). Detailed information and experimental conditions can be found in our previous work [24].

2.3. Electrochemical tests

The electrochemical tests were performed on an electrochemical analyzer (CHI 660a, China) [25]. The working electrode was prepared with the established procedure [26]. The active material on the electrode is 80 mg. The Ag/AgCl and platinum foil were enlisted as reference and counter electrode, respectively.

3. RESULTS AND DISCUSSION

3.1. Characteristics of composite samples

Figure 1 shows the XRD patterns of Co-Ni-B and Co-Ni-Mn-O. No obvious peak can be observed in the pattern of Co-Ni-B, demonstrating an amorphous nature [27]. After the oxidation, Co-Ni-Mn-O shows two additional peaks at 35.5° and 58.9° , which can be indexed to the (101) and (211) of MnO_2 (PDF No. 04-0591). These results suggest that potassium permanganate was reduced to MnO_2 . However, Co and Ni oxides do not show obvious featured peaks, possibly because of the overlapping of MnO_2 .

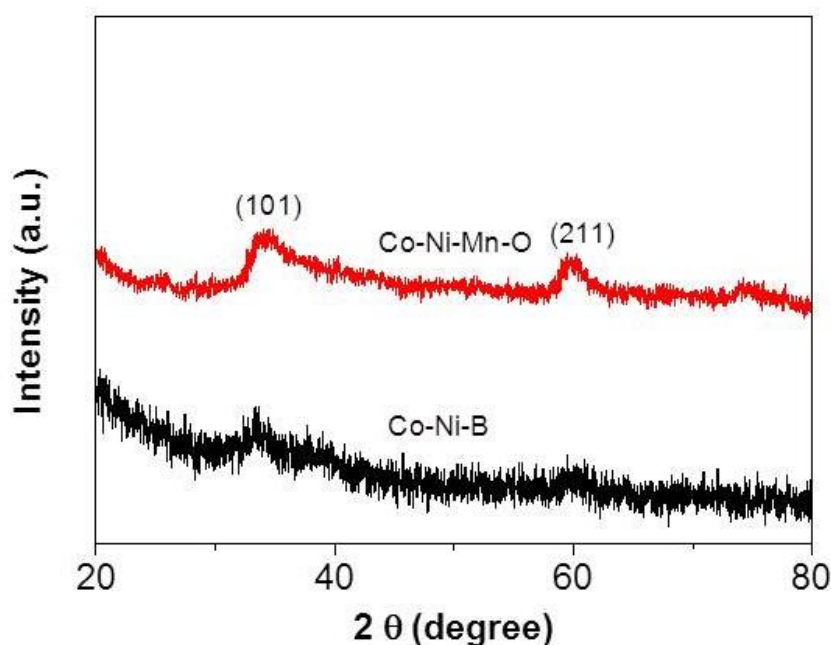


Figure 1. XRD patterns of Co-Ni-B and Co-Ni-Mn-O.

The surface morphologies of the sample were observed by SEM. As shown in Figure 2, Co-Ni-B is composed of porous nanosheets (Figure 2a,b). It has shown that Co-B based alloy synthesized under acetonitrile solution can form nanosheets structure. The nanosheets can be easily accessed by the electrolyte ions and thus improve the electron transfer. After the deposition of MnO_2 nanoparticles on the Co-Ni-B nanosheets, the surface of the sample became rough (Figure 2c,d). The aggregated MnO_2 nanoparticles were covered on the Co-Ni-B nanosheets.

More detailed morphological information of the samples was observed by TEM. The Co-Ni-B nanosheets shows wrinkled surface (Figure 3a,b). The deposited MnO_2 nanoparticles were uniformly distributed on Co-Ni-B nanosheets (Figure 3c,d). The size of the MnO_2 is about 10 nm.

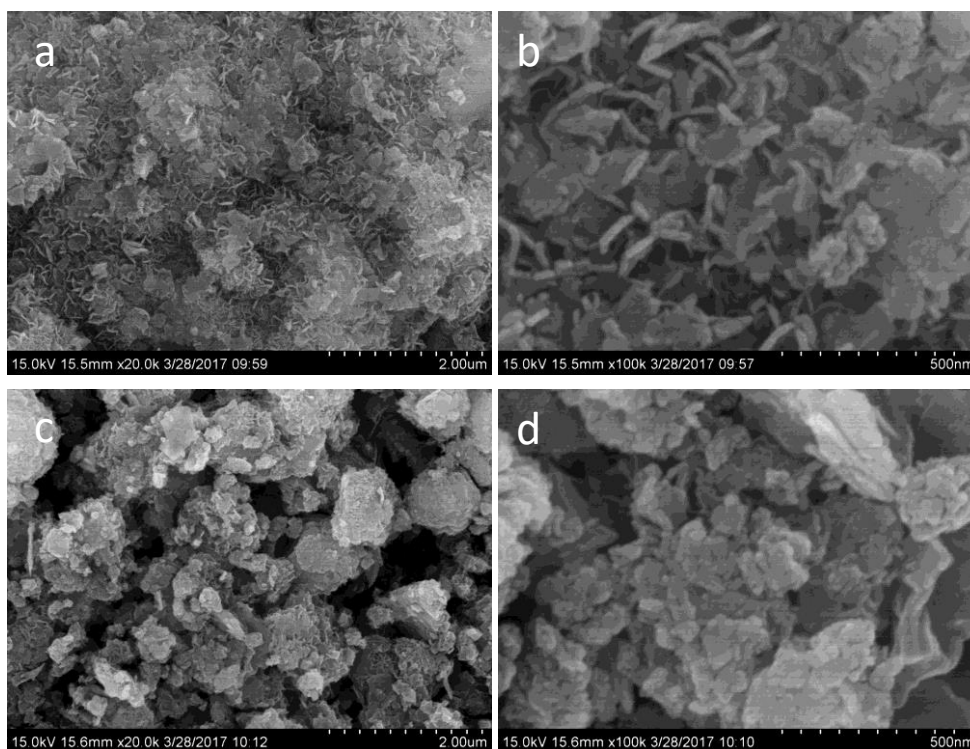


Figure 2. SEM images of Co-Ni-B (a,b) and Co-Ni-Mn-O (c,d).

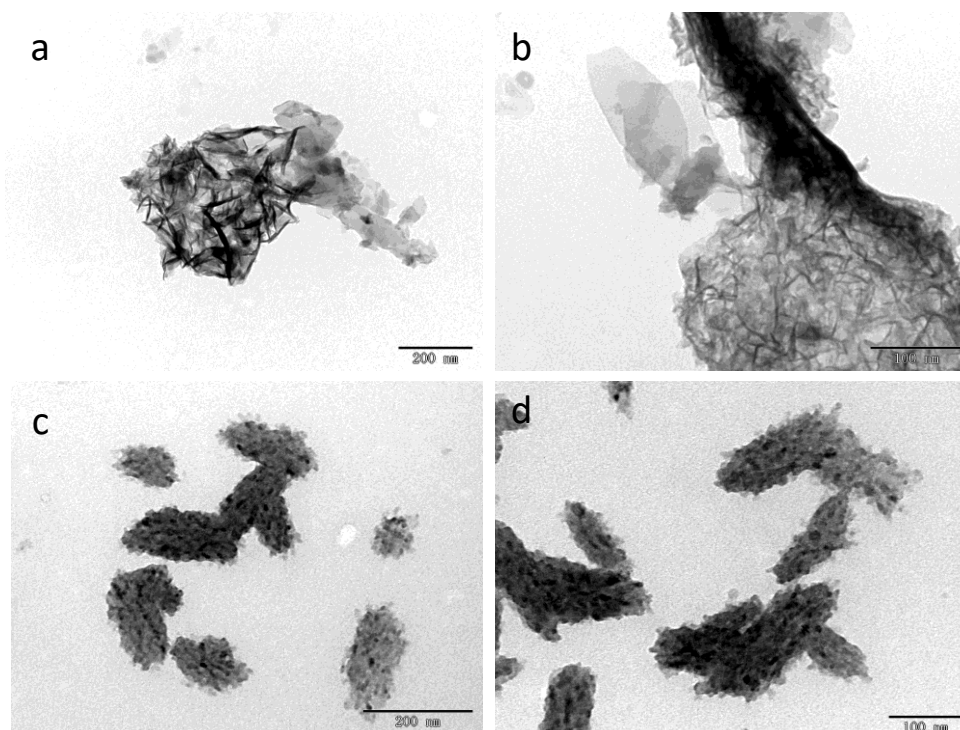


Figure 3. TEM images of Co-Ni-B (a, b) and Co-Ni-Mn-O (c,d).

The chemical states of the element in the Co-Ni-Mn-O composite were further conducted by XPS. Figure 4a shows the full survey spectrum of Co-Ni-Mn-O. The Co-Ni-Mn-O consists of five

elements Co, Ni, Mn, O and B, and the peaks are located at 781 eV (Co 2p), 856 eV (Ni 2p), 643 eV (Mn 2p), 531 eV (O 1s) and 192 eV (B1s). B is also detected in Co-Ni-Mn-O, which is originated from NaBH₄. For the high resolution XPS of Co2p (Figure 4b), two obvious peaks observed at 781.1 and 796.8 eV represents Co 2p_{3/2} and Co 2p_{1/2} respectively. The peaks at 787.4 and 803.2 eV are indexed to the satellite peaks of Co 2p_{3/2} and Co 2p_{1/2}. These results are consistent with previous reports [28]. The separation of Co 2p_{1/2} and Co 2p_{3/2} is over 15 eV, indicating the coexistence of Co²⁺ and Co³⁺ [29]. In Figure 4c, the XPS spectrum of Ni 2p can also be fitted into two spin-orbit doublets (873.5 and 855.8 eV) and two shakeup satellites (861.6 and 880.1 eV). The main Ni 2p_{3/2} peak is close to 854.9 eV for Ni²⁺ but much lower than 857.1 eV for Ni³⁺, suggesting valence state of Ni is +2, For the high resolution XPS of Mn2p (Figure 4d), two broad peaks of Mn 2p_{3/2} and 2p_{1/2} are at 642.7 and 653.9 eV, respectively, demonstrating that Mn⁴⁺ ions were dominant in the products. These results demonstrate the oxides presented in Co-Ni-Mn-O are Co₃O₄, NiO, and MnO₂.

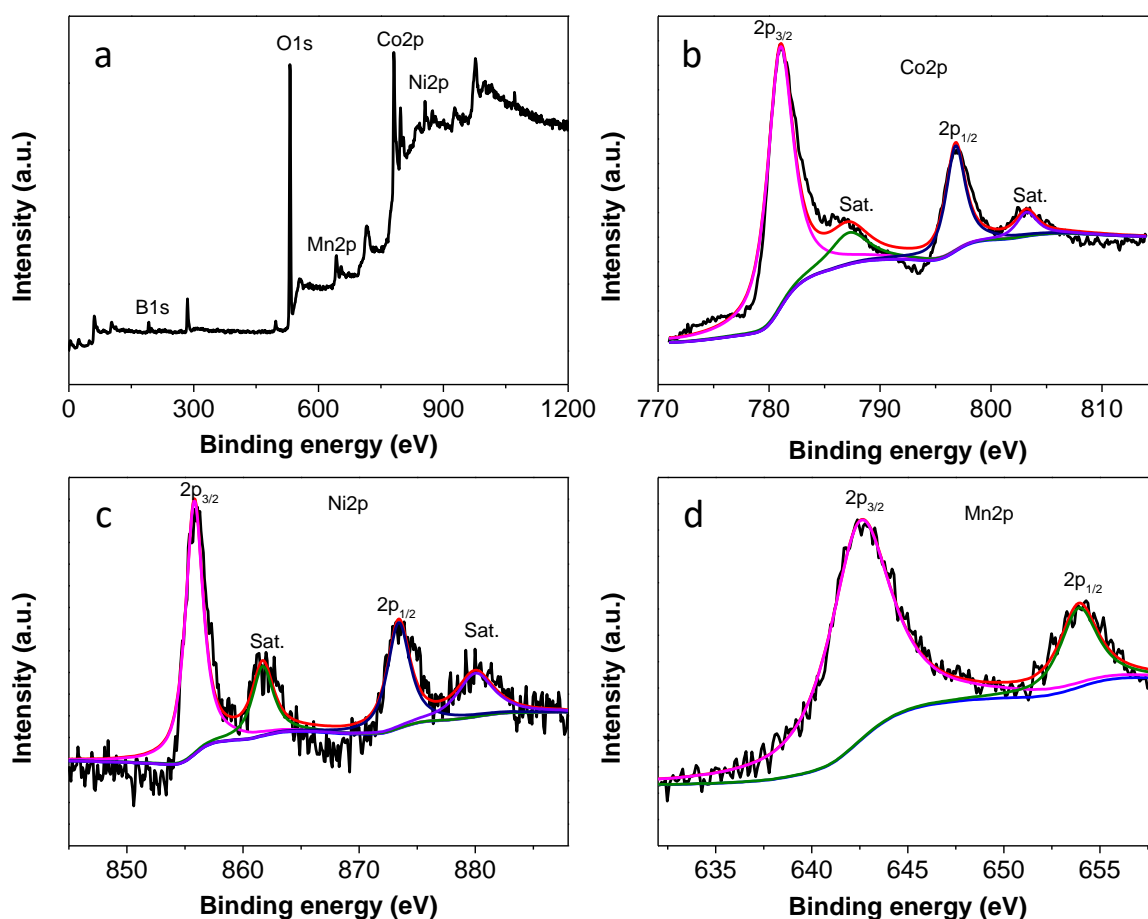


Figure 4. XPS spectra of Co-Ni-Mn-O, (a) Survey, (b) Co2p, (c) Ni2p, (d) Mn2p.

3.2 Electrochemical characterization of Co-Ni-Mn-O

The electrochemical measurements were conducted in 6 M KOH solution. Figure 5 shows the galvanostatic charge-discharge (GCD) curve of Co-Ni-Mn-O and Co-Ni-B. The two electrodes were

charged and discharged in a potential window ranged from -0.4 to 0.4 V. The Co-Ni-Mn-O electrode shows longer discharging time than Co-Ni-B electrode, indicating a higher specific capacitance. The charging and discharging curves are distorted lines, demonstrating a typical feature of pseudocapacitor. The calculated specific capacitances for Co-Ni-Mn-O and Co-Ni-B electrode are 811.8 and 436.9 F g⁻¹, respectively. The obtained capacitance for Co-Ni-Mn-O is higher than most MnO₂-based electrodes, indicating its superiority.

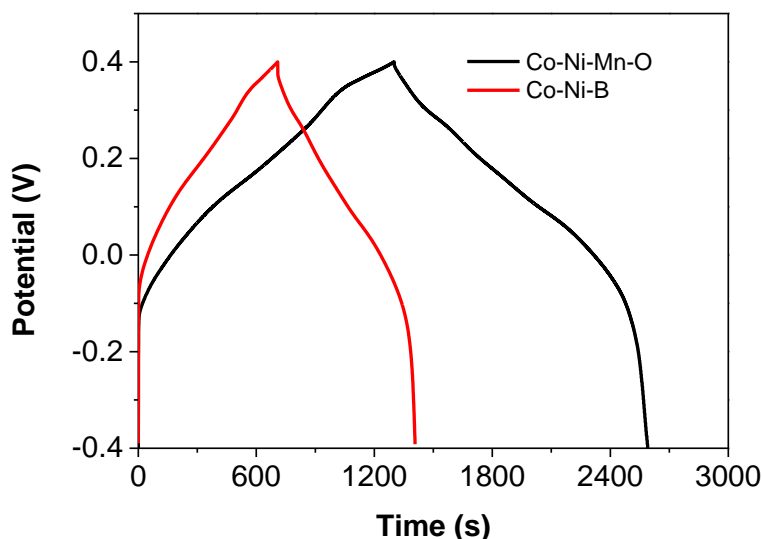


Figure 5. The GCD curves for Co-Ni-Mn-O and Co-Ni-B electrode at 0.5 A g⁻¹.

Table 1. Comparison of specific capacitance of Co-Ni-Mn-O with reported results

Sample	Specific capacitance (F g ⁻¹)/current density (A g ⁻¹)	Reference
Mn-iron-oxide	224.6/1	[30]
MnO ₂ /MXene/CC	511.2/1	[31]
MnO ₂ /SC	231/0.5	[32]
MnO ₂ /rGO	234.8/0.1	[33]
H-MnO ₂ /ACC-100	400/0.5	[34]
Ni-Co-Mn oxide	715.1/1	[35]
Fe-doped MnO ₂	627.3/1	[36]
Mn ₃ O ₄	260/1	[37]
Co-Ni-Mn-O	811.8/0.5	This work

The impedance is a useful tool to investigate the electrochemical reaction on the electrode [38, 39]. Figure 6 shows the Nyquist plots of Co-Ni-Mn-O and Co-Ni-B electrode. The calculated charge-

transfer resistances (R_{ct}) for the Co-Ni-Mn-O and Co-Ni-B electrode are 0.8 and 4 ohm respectively. The charge-transfer resistance of Co-Ni-Mn-O is much smaller than Co-Ni-B, which indicates the fastest charge transfer in Co-Ni-Mn-O. Besides, in the region of the low frequency, the curves of Co-Ni-Mn-O are almost vertical to the X axis, proving a lesser diffusive resistance of materials.

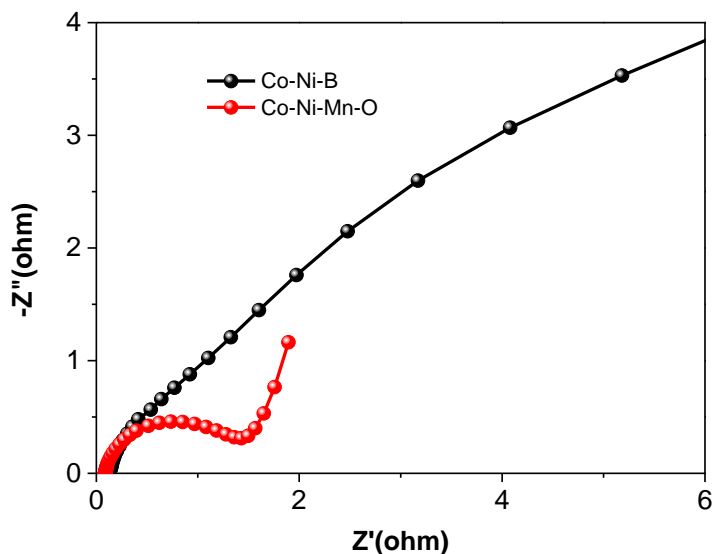


Figure 6. Nyquist curves of Co-Ni-Mn-O and Co-Ni-B electrode.

Figure 7 shows the cyclic voltammetry (CV) curves of Co-Ni-Mn-O with different scan rates. A pair of redox peaks was observed in the CV curves, indicating the Faradic reactions take place on the electrode. When the scan rate increased from 5 to 120 mV s^{-1} , the separations of the peak potential do not increase too much, indicating a fast electron transfer and good stability [40].

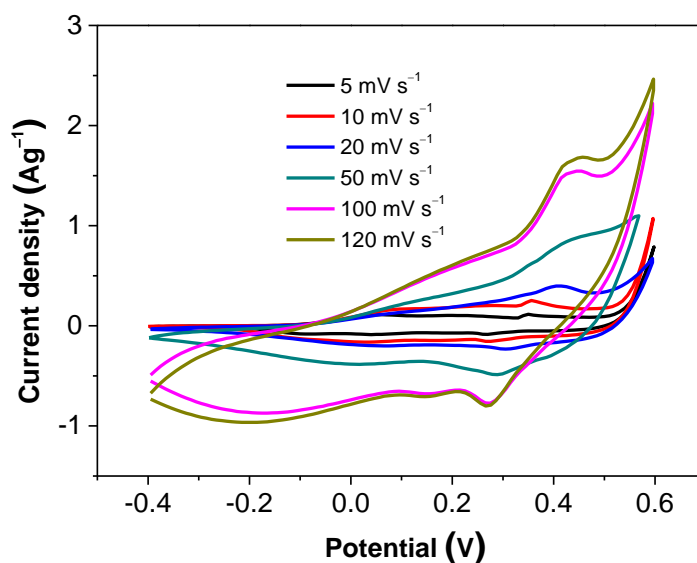


Figure 7. CV curves of Co-Ni-Mn-O at scan rates from 5 to 120 mV s^{-1} .

The rate capability is a crucial factor for supercapacitors. The rate capability of the Co-Ni-Mn-O electrode was investigated by charging-discharging the electrode at different current density. Figure 8 shows the GCD curves of Co-Ni-Mn-O at 0.5, 1, 2, 4, 10 A g⁻¹. The calculated specific capacitances of the electrode are 811.8, 746.4, 702.7, 647.5, 603.2 F g⁻¹ at 0.5, 1, 2, 4, 10 A g⁻¹, respectively. The capacitance at 10 A g⁻¹ can retain 74.3% of that at 0.5 A g⁻¹, demonstrating excellent high rate capability.

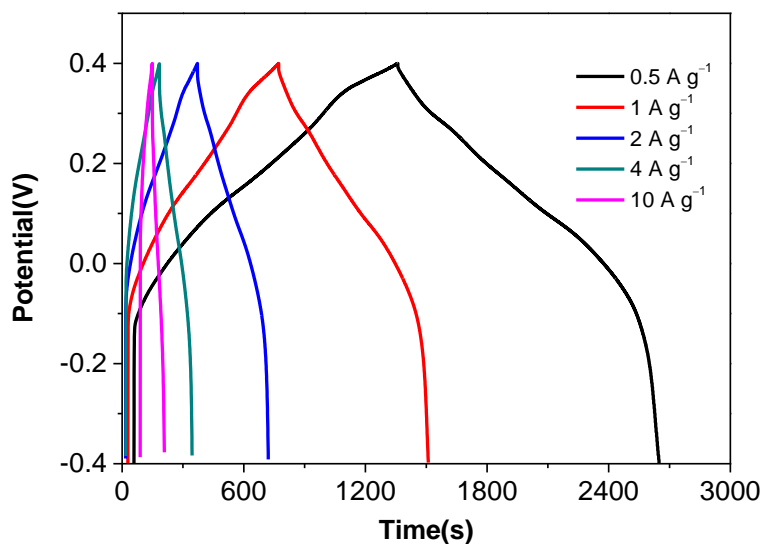


Figure 8. GCD curves of Co-Ni-Mn-O at 0.5, 1, 2, 4, 10 A g⁻¹.

The stability determines the feasibility of the application of supercapacitors directly. Therefore, to check the potential application of the Co-Ni-Mn-O electrode, the cycling stability was studied by charging-discharging the electrode for 3000 cycles. As revealed in Figure 9. After 3000 cycles running, the Co-Ni-Mn-O electrode can keep 86.5 % capacitance of its initial stage, suggesting a remarkable stability.

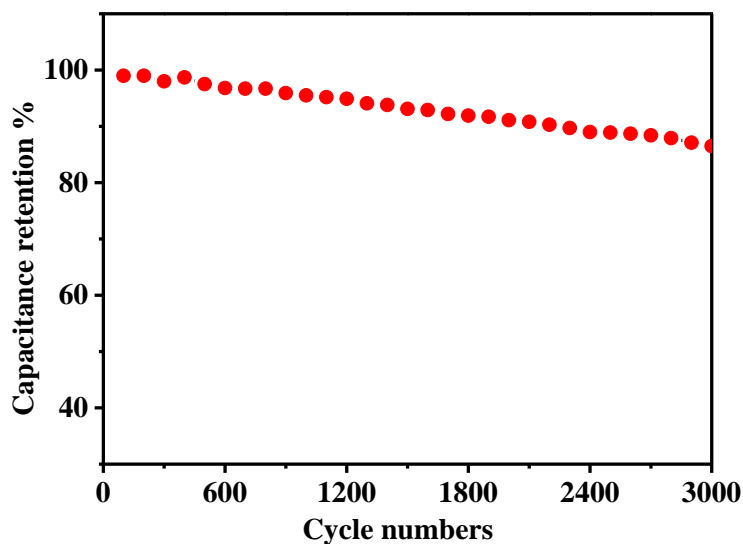


Figure 9. Cycling stability of Co-Ni-Mn-O electrode at 1 A g⁻¹.

4. CONCLUSIONS

A simple way to prepare Co-Ni-Mn-O ternary oxides was developed in this study. The ternary oxides were identified as Co_3O_4 , NiO and MnO_2 . The ternary oxides demonstrate excellent electrochemical properties, which is suitable for fabrication the high-performance supercapacitor electrode. A high capacitance of 811.8 F g^{-1} can be achieved at 1 A g^{-1} . Furthermore, the rate capability and stability of the Co-Ni-Mn-O electrode are found to be excellent. These features enable the Co-Ni-Mn-O electrode to be a good candidate for energy storage devices.

ACKNOWLEDGEMENTS

This work was supported by the Guangxi undergraduate innovation and entrepreneurship training program (201810595017) and GXNSF (2017AD23029, 2017GXNSFDA198018).

References

1. Y. Zhang, Q. Yi, Z. Deng, X. Zhou, H. Nie, *Catal. Lett.*, 148 (2018) 1190-1201.
2. H. Peng, Z. Mo, S. Liao, H. Liang, L. Yang, F. Luo, H. Song, Y. Zhong, B. Zhang, *Sci. Rep.*, 3 (2013)1765.
3. Z. Wang, X. Luo, B. Zheng, L. Huang, C. Hang, Y. Jiao, X. Cao, W. Zeng, R. Yun, *Eur. J. Inorg. Chem.*,11 (2018) 1309-1314.
4. H. Song, A. Tang, G. Xu, L. Liu, M. Yin, Y. Pan, *Int. J. Electrochem. Sci.*, 13 (2018) 4720-4730.
5. H. Song, A. Tang, G. Xu, L. Liu, Y. Pan, M. Yin, *Int. J. Electrochem. Sci.*, 13 (2018) 6708-6716.
6. Z.L. Deng, Q.F. Yi, G. Li, Y. Chen, X.K. Yang, H.D. Nie, *Electrochim. Acta*, 279 (2018) 1-9.
7. Z. Deng, Q. Yi, Y. Zhang, H. Nie, *J. Electroanal. Chem.*, 803 (2017) 95-103.
8. C. Wang, Z. Ma, Y. Wang, C. Lu, *J. Electrochem. Soc.*, 163 (2016) A1157-A1163.
9. Q. Yi, H. Chu, M. Tang, Y. Zhang, X. Liu, Z. Zhou, H. Nie, *Fuel Cells*, 14 (2014) 827-833.
10. G.R. Xu, Y. Wen, X.P. Min, W.H. Dong, A.P. Tang, H.S. Song, *Electrochim. Acta*, 186 (2015) 133-141.
11. Q. Yi, H. Chu, M. Tang, Z. Yang, Q. Chen, X. Liu, *J. Electroanal. Chem.*, 739 (2015) 178-186.
12. Q. Yi, H. Chu, Q. Chen, Z. Yang, X. Liu, *Electroanal.*, 27 (2015) 388-397.
13. K. Deng, C. Li, X. Qiu, J. Zhou, Z. Hou, *Electrochim. Acta*, 174 (2015) 1096-1103.
14. K. Deng, C. Li, X. Qiu, J. Zhou, Z. Hou, *J. Electroanal. Chem.*, 755 (2015) 197-202.
15. C. Xiang, Y. Liu, Y. Yin, P. Huang, Y. Zou, M. Fehse, Z. She, F. Xu, D. Banerjee, D. Hermida Merino, A. Longo, H.B. Kraatz, D.F. Brougham, B. Wu, L. Sun, *ACS Appl. Energy Mater.*, 2 (2019) 3389-3399.
16. Q. Yi, Q. Chen, *Electrochim. Acta*, 182 (2015) 96-103.
17. L. Yi, W. Wei, C. Zhao, C. Yang, L. Tian, J. Liu, X. Wang, *Electrochim. Acta*, 158 (2015) 209-218.
18. Q. Yi, Y. Zhang, X. Liu, Y. Yang, *Sci. Chi. Chem.*, 57 (2014) 739-747.
19. C. Lamiel, V.H. Nguyen, D.R. Kumar, J.J. Shim, *Chem. Eng. J.*, 316 (2017) 1091-1102.
20. Q. Ma, W. Hu, D. Peng, R. Shen, X. Xia, H. Chen, Y. Chen, H. Liu, *J. Alloys Compd.*, 803 (2019) 866-874.
21. L. Luo, B. He, W. Kong, Z. Wang, *J. Alloys Compd.*, 705 (2017) 349-355.
22. N.K. Alam Venugopal, J. Joseph, *J. Power Sources*, 305 (2016) 249-258.
23. Y. Zou, Y. Gao, C. Xiang, H. Chu, S. Qiu, E. Yan, F. Xu, C. Tang, L. Sun, *Metals*, 6 (2016) 154.
24. Y. Yin, C. Xiang, H. Chu, H. Zhang, X. Fen, E. Yan, L. Sun, C. Tang, Y. Zou, *Appl. Surf. Sci.*, 460 (2018) 25-32.
25. S. Chen, S. Liu, A. Wen, J. Zhang, H. Nie, J. Chen, R. Zeng, Y. Long, Y. Jin, R. Mai, *Electrochim. Acta*, 271 (2018) 312-318.
26. Y. Zou, C. Cai, C. Xiang, P. Huang, H. Chu, Z. She, F. Xu, L. Sun, H.-B. Kraatz, *Electrochim.*

- Acta*, 261 (2018) 537-547.
27. Y. Zou, Y. Gao, P. Huang, C. Xiang, Ha. Chu ,Sh. Qiu , E. Yan, F. Xu, L. Sun, *Metals*, 7 (2017) 365.
 28. Y. Xia, G. Wang, X. Zhang, B. Wang, H. Wang, *Electrochim. Acta*, 220 (2016) 643-653.
 29. Y. Liu, Y. Jiao, B. Yin, S. Zhang, F. Qu, X. Wu, *J. Mater. Chem. A*, 3 (2015) 3676-3682.
 30. K. Li, X. Liu, T. Zheng, D. Jiang, Z. Zhou, C. Liu, X. Zhang, Y. Zhang, D. Losic, *Chem. Eng. J.*, 370 (2019) 136-147.
 31. H. Zhou, Y. Lu, F. Wu, L. Fang, H. Luo, Y. Zhang, M. Zhou, *J. Alloys Compd.*, 802 (2019) 259-268.
 32. X.-P. Chen, J. Wen, C.-X. Zhao, Y.-T. Li, N. Wang, *Chemistryselect*, 3 (2018) 9301-9307.
 33. Y. Chen, J. Zhang, M. Li, C. Yang, L. Zhang, C. Wang, H. Lu, *Electrochim. Acta*, 292 (2018) 115-124.
 34. J. Zhang, J. Sun, T.A. Shifa, D. Wang, X. Wu, Y. Cui, *Chem. Eng. J.*, 372 (2019) 1047-1055.
 35. S. Chen, G. Yang, H. Zheng, *Electrochim. Acta*, 220 (2016) 296-303.
 36. Q. Gao, J. Wang, B. Ke, J. Wang, Y. Li, *Ceram. Int.*, 44 (2018) 18770-18775.
 37. B. Li, X. Zhang, J. Dou, C. Hu, *Ceram. Int.*, 45 (2019) 16297-16304.
 38. K. Deng, C. Li, H. Huang, X. Li, *Sens. Actuators B-Chem.*, 238 (2017) 1302-1308.
 39. C. Li, X. Qiu, K. Deng, Z. Hou, *Anal. Meth.*, 6 (2014) 9078-9084.
 40. M. Tang, Y. Yang, S. Zhang, J. Chen, J. Zhang, Z. Zhou, Q. Liu, *Inorg. Chem.*, 57 (2018) 277-287.

© 2019 The Authors. Published by ESG (www.electrochemsci.org). This article is an open access article distributed under the terms and conditions of the Creative Commons Attribution license (<http://creativecommons.org/licenses/by/4.0/>).